Available online at www.sciencedirect.com

SCIENCE DIRECT®

Applied Surface Science 233 (2004) 180–190

applied surface science

www.elsevier.com/locate/apsusc

The growth morphology and crystallinity of electroless NiP deposition on silicon

Ting-Kan Tsai[a,b,*], Chuen-Guang Chao[a]

[a]Department of Materials Science and Engineering, National Chiao Tung University, Hsinchu 300, Taiwan, ROC

[b]Department of Materials Science and Engineering, National Huwei Institute of Technology, Huwei, Yunlin 632, Taiwan, ROC

Received 17 January 2004; received in revised form 10 March 2004; accepted 10 March 2004

Available online 17 April 2004

Abstract

The growth morphology and crystallinity of the electroless NiP deposited on Si substrate pretreated by $SnCl_2$/HCl and $PdCl_2$/HCl solutions is studied using transmission electron microscope (TEM), field emission scanning electron microscope (FESEM), and energy dispersive X-ray spectrum (EDS). Combining cross-sectional and surface observations show that the reaction mechanism of electroless NiP on Si is an electrochemical mechanism and the deposits are composed of a columnar structure grown along the vertical direction of the substrate surface. The phosphorus content does not have influence on the growth morphology but affects the crystallinity of the deposits. The crystallinity of the deposits is directly observed by the lattice image using high-resolution transmission electron microscope (HRTEM). The as-deposited NiP with 10.7 at.% P possesses good crystallinity and consists of Ni nanocrystal about 4–8 nm distributed randomly in the deposits. The size of nanocrystal in the deposits with 15.2 at.% P is about 2–5 nm. The deposits with 20.3 at.% P have a smaller order range and the size of nanocrystal is under 1.5 nm. The grain size decreases as the phosphorus content increases.
© 2004 Elsevier B.V. All rights reserved.

Keywords: Electroless NiP; Growth morphology; Crystallinity; Si

1. Introduction

Since the electroless nickel plating technique was introduced by Brenner and Riddell in 1946 [1], the electroless plating technique have been applied in electronics, machinery, automotive, aerospace, oil and gas, and chemical engineering industries, due to its simplicity in operation, low cost in equipment, and mass production in many suitable case [2,3]. In the past several years, electroless deposition was widely used in the electronic and semiconductor-device industries for delineating semiconductor junctions [4,5], making ohmic contact [6], filling vias [7], and patterning printed circuit boards [8]. Recently, the investigations of nanostructures fabricated on silicon wafer for the development of nano-devices have been reported successively [9–11]. The electroless plating is one of the most attractive manufacturing methods in mass-production of nanostructures [12].

The electroless NiP is an important electroless deposition alloy in electronic and semiconductor-device industries due to its excellent corrosion resistance, solderability, thermal stability, and electrical property. Several researchers have investigated the

* Corresponding author. Tel.: +886-5-632-9643x621; fax: +886-5-636-1981.
E-mail address: dktsai@sunws.nhit.edu.tw (T.-K. Tsai).

0169-4332/$ – see front matter © 2004 Elsevier B.V. All rights reserved.
doi:10.1016/j.apsusc.2004.03.014

electroless NiP deposition on silicon wafer. The first attempt to deposit electroless nickel for ohmic contact onto Si was made by Sullivan and Eigler in 1957 [6]. Iwasa et al. [4] made a study of the electroless nickel deposition on Si wafer with *p–n* junctions using conventional solutions. Singh and Mitra [13] investigated the influence of pH and bath temperature on NiP/Si contact resistance. Don et al. [14] studied the structure and electrical properties of chemical deposited Ni/Si contacts. In more recent years, Lynch et al. [15] studied the interfacial electrical properties of electroless NiP contact on silicon. Rohan et al. [16] deposited the NiP on Si wafer as a final barrier/bonding layer material for microelectronics applications. Lin and Chen [17] deposited electroless NiP on silicon wafer simulating the UBM of flip chip solder bump. Wang et al. [18] and Kordás et al. [19] made the study about the selective deposition of NiP on silicon under laser irradiation. Takano and co-workers [20,21] investigated the mechanism of the electroless nickel deposition on Si wafer in aqueous alkaline solution for fabricating fine metal dot arrays. We have investigated the catalytic effect of electroless NiP alloy on Si wafer for the growth of carbon nanofibers [22]. As mentioned above, there have numerous reports on the study of the electroless NiP deposits on Si substrate. In most of these studies, the applications of the electroless NiP deposited on Si wafer were investigated. Only little investigation about the growth morphology and crystallinity of the electroless NiP deposits on the sensitized and activated Si substrate was published. Several fundamental problems on the growth morphology and reaction mechanism of the electroless NiP on Si are not completely clear. Thus, a more detailed examination for the growth morphology and crystallinity of the electroless NiP deposition on Si pretreated by $SnCl_2$/HCl and $PdCl_2$/HCl is required.

In general, the investigation on the growth mechanism of the electroless NiP deposition was often observed by the surface morphology. Lack of the information about the lateral morphology made the growth mechanism of the electroless NiP still controversial in some aspects. The crystallinity of the NiP deposit was always determined by the electron diffraction and X-ray diffraction. These conventional methods are short of the direct evidences to distinguish the amorphous or nanocrystal in the deposits. In this present study, we made a thorough investigation on the growth morphology and crystallinity of electroless NiP with various phosphorus contents deposited on silicon wafer sensitized by $SnCl_2$/HCl and activated by $PdCl_2$/HCl. Both the surface topography and the cross-sectional image were used to study the growth morphology of the electroless NiP deposited on Si. The crystallinity of the as-deposited NiP film was directly identified by the lattice image using high-resolution transmission electron microscope (HRTEM).

2. Experimental

The substrates for electroless plating used in this study were p-type (1 0 0) silicon wafer (resistivity about 1–20 Ω cm). The silicon wafers were degreased by ultrasonic vibration in acetone. The degreased specimens were cleaned with a solution mixed one part of H_2SO_4 and one part of H_2O_2 for 15 min and then etched in 10% HF aqueous solution to remove oxide. Prior to the electroless plating process, it is necessary to sensitize and activate the depositing surface of silicon wafer using $SnCl_2$/HCl solution (40 g/l $SnCl_2$ + 3 ml/l HCl) and $PdCl_2$/HCl solution (0.15 g/l $PdCl_2$ + 3 ml/l HCl). The etched specimens were sensitized by immersion in $SnCl_2$/HCl solution for 2 min and activated by immersion in $PdCl_2$/HCl solution for 30 s. After each pretreatment step, as mentioned above, the specimens were rinsed in distilled water.

The plating solution used in this work was composed of a mixture of $NiSO_4$, NaH_2PO_2, $Na_2C_4H_4O_4$, and $Pb(NO_3)_2$, where $NiSO_4$ as the main nickel sources, NaH_2PO_2 as the reducing agent, $Pb(NO_3)_2$ as the stabilizing agent, and $Na_2C_4H_4O_4$ as buffer and complex agent for nickel. The composition of plating solutions and the experimental condition are list in Table 1. The pH of the plating solution was adjusted with NaOH aqueous solution.

Transmission electron microscope (TEM) (JEOL Ltd., JEM-2010) was utilized to observe the cross-sectional image of the electroless NiP film. The surface topography of the deposit was observed by field emission scanning electron microscope (FESEM) (JEOL Ltd., JSM-6330FEM). The elemental analysis of the deposits was identified by a TEM equipped with an Oxford Link energy dispersive X-ray spectrum

Table 1
The composition of plating solution and experimental condition for electroless NiP plating

Chemicals	Concentration (g/l)
$NiSO_4 \cdot 6H_2O$	20
$NaH_2PO_2 \cdot H_2O$	27
$Na_2C_4H_4O_4 \cdot 6H_2O$	16
$Pb(NO_3)_2$	1 ppm
pH = 4.2, 4.8, 5.2	Temperature 70 °C

(EDS). The Cliff–Lorimer ratio technique was employed as the chemical composition quantification method. The ratio standard element and line are silicon and K series. Ten composition analysis points were measured at least for one sample. The lattice image of the deposits obtained at different pH values was characterized by HRTEM (JEOL Ltd., JEM-2010).

3. Results and discussion

3.1. Pretreatment

Fig. 1a is the TEM cross-sectional image of the Si substrate pretreated by immersion in $SnCl_2$/HCl solution for 2 min. The sensitization layer is continuous and covers the substrate surface uniformly. The thickness of the sensitization layer is approximately

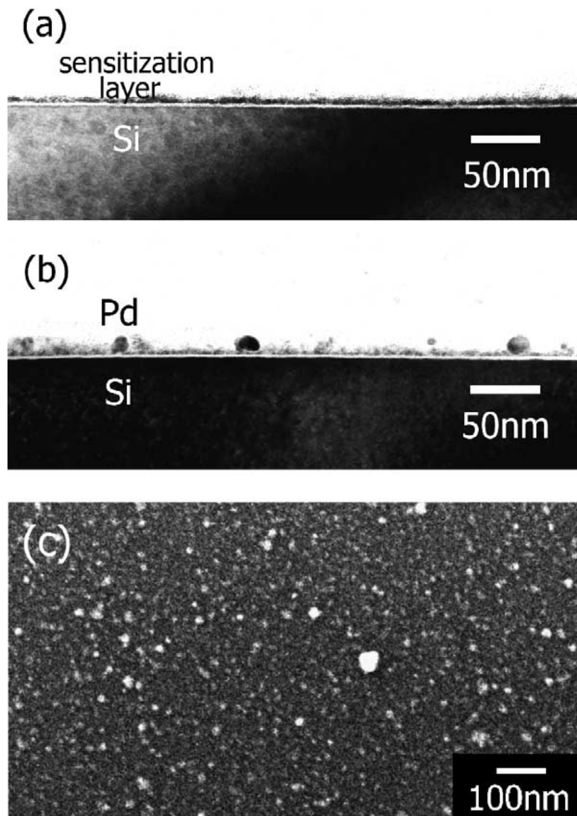

Fig. 1. (a) TEM cross-section image of the Si substrate pretreated by immersion in $SnCl_2$ solution for 2 min. (b) TEM cross-section image of the Si substrate pretreated by immersion in $SnCl_2$ solution for 2 min and in $PdCl_2$ solution for 30 s. (c) FESEM surface topography image of the Si substrate pretreated by immersion in $SnCl_2$ solution for 2 min and in $PdCl_2$ solution for 30 s.

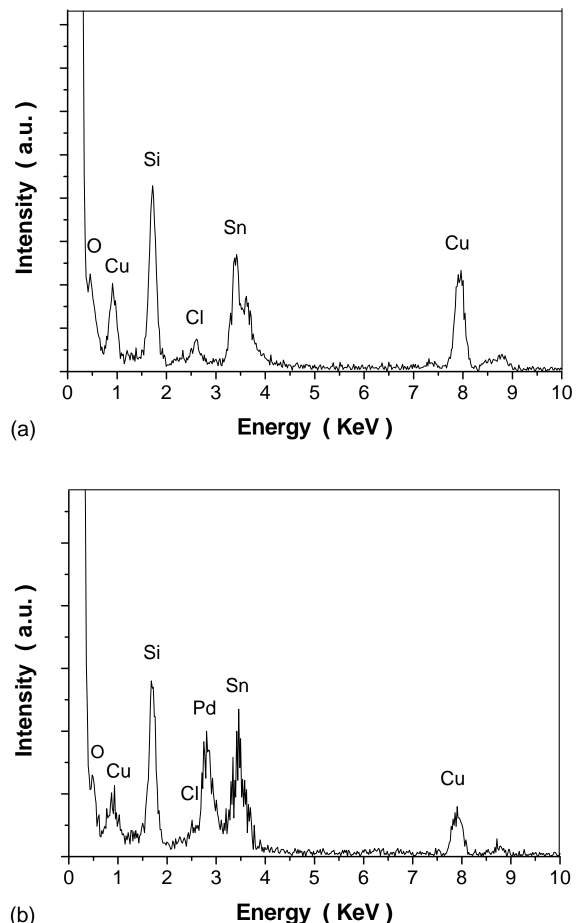

Fig. 2. EDS spectra of (a) the sensitized specimen and (b) the activated specimen.

3–5 nm. In Fig. 1a, we also find that there is an amorphous layer of which the thickness is about 2–3 nm between the Si substrate and the sensitization layer. Fig. 2a is the EDS spectrum of the sensitized specimen. The EDS analysis reveals that the sensitization layer consists mainly of Sn and Cl. The signal of Cu is probably from the copper grid. The existence of O peak in the EDS spectrum implies the amorphous layer in Fig. 1a is SiO_2. The SiO_2 layer is maybe produced in distilled water rinse before the sensitization treatment.

Fig. 1b and c is the TEM cross-sectional image and the FESEM surface topography of the Si substrate pretreated by immersion in $SnCl_2$/HCl solution for 2 min and in $PdCl_2$/HCl solution for 30 s in sequence, respectively. The activation pretreatment is appeared to produce small catalytic particles exhibited island form dispersed on the sensitization layer. These catalytic particles with different size sparsely and unevenly dispersed on the sensitized surface of Si substrate. The size of these catalytic particles is approximately 5–30 nm and some larger catalytic particles with 50–70 nm have been also observed. The EDS analysis of the activated specimen, as seen in Fig. 2b, indicates that the signals of Sn and Pd are presented in the spectrum and confirms that the catalytic particles on the sensitization layer are Pd particles.

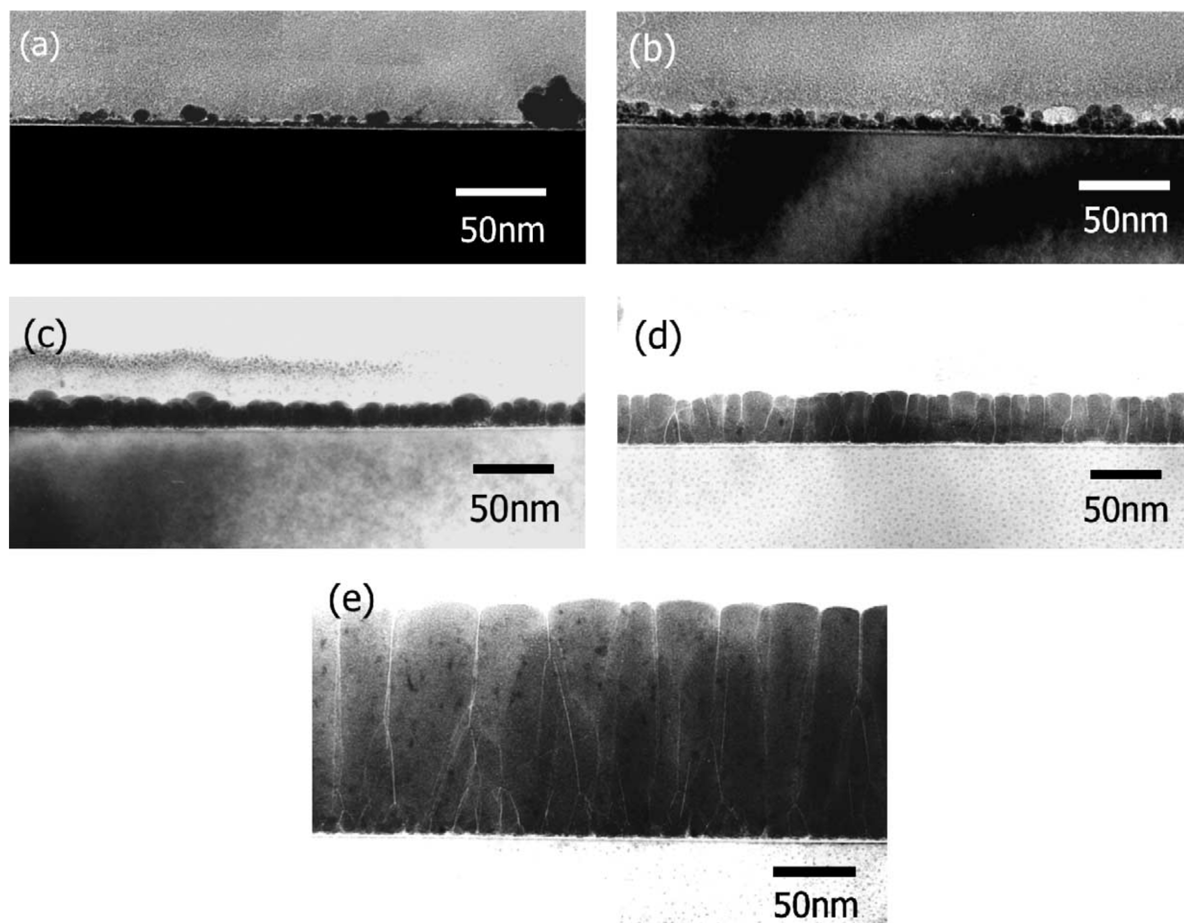

Fig. 3. TEM cross-section images of the electroless NiP alloy plating for various deposition time deposited at pH 5.2: (a) 2 s; (b) 4 s; (c) 6 s; (d) 15 s; and (e) 60 s.

3.2. Growth morphology

In Figs. 3 and 4, we present the growth morphology of the electroless NiP deposits on Si substrate in different deposition stage. The pH value of the plating solution is 5.2 and the average phosphorus content of the deposit is 10.7 at.% determined by EDS. Fig. 3a–e illustrates the TEM cross-sectional image of the deposit plating for 2, 4, 6, 15, and 60 s, respectively. Fig. 4a–e shows the corresponding FESEM surface topographies of these deposits. The deposits plating for 2 s, as shown in Figs. 3a and 4a, have a similar morphology as the activated specimens (as see in Fig. 1b and c). We cannot determine whether the Ni has been deposited on the substrate from these observations. Fig. 5a is the EDS spectrum of the deposits for 2 s. We can find the signals of Ni, P, Pb, Sn and Pd presented in the EDS spectrum. The presence of Ni peak in the EDS spectrum indicates that the Ni particles have been deposited on Si in the deposition duration. The signals of P, Pb and Sn appeared in the EDS spectrum reveals that the P and Pb co-precipitated with Ni in the initial stage of deposition and the sensitization layer still existed on the substrate.

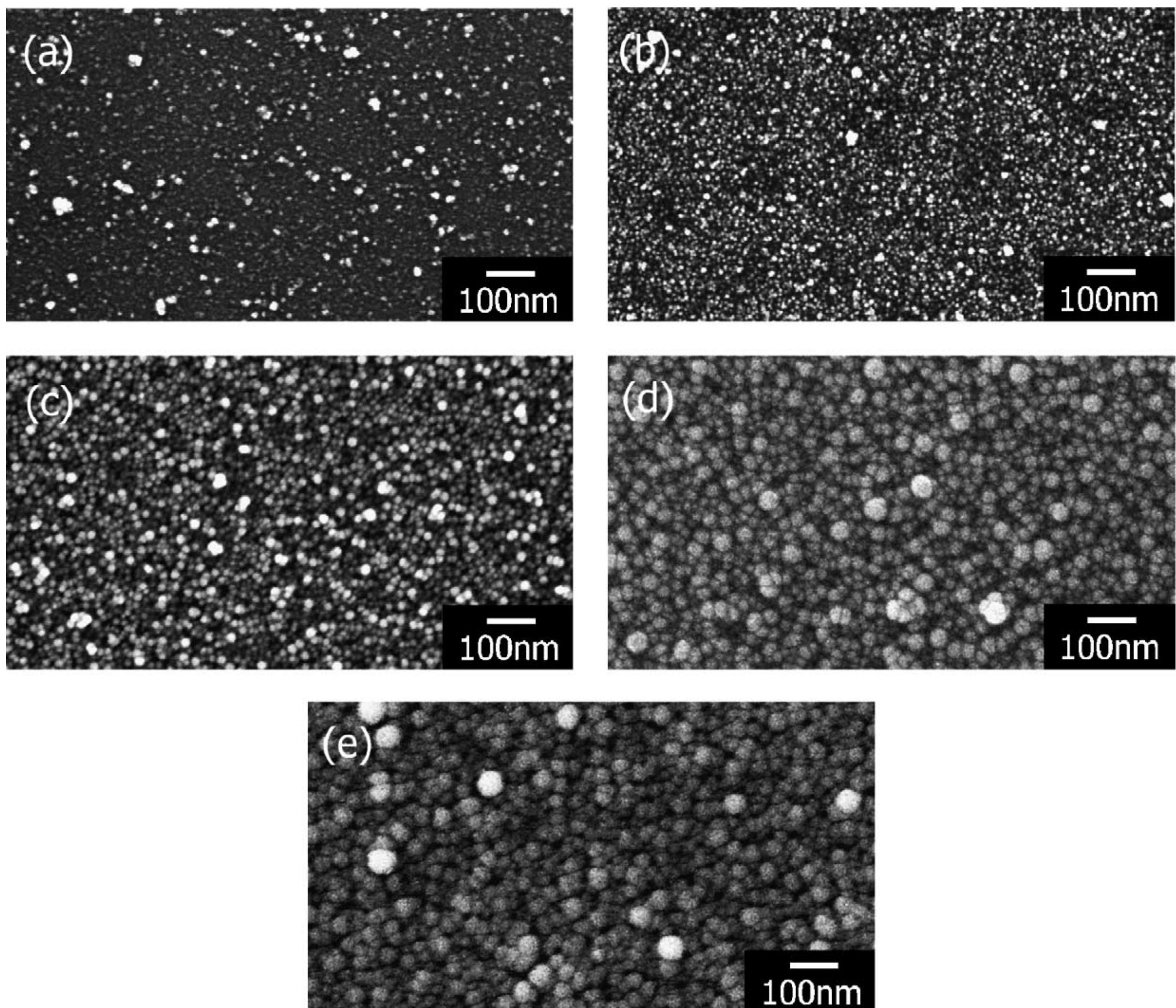

Fig. 4. FESEM surface topography images of the electroless NiP alloy plating for various deposition time deposited at pH 5.2: (a) 2 s; (b) 4 s; (c) 6 s; (d) 15 s; and (e) 60 s.

Another phenomenon worthy of mentioning is that the peak of Ni presents together with the peak of Pd in the EDS analysis of the deposits for 2 s. This phenomenon implies that the initial deposition of NiP related to the presence of Pd. The deposition of Ni can occur at any place where the electrons can be offered for Ni ions reduced to Ni metal. The Pd particles act as charge exchange and hydrogen evolution centers, thus the initial deposition is easily occurred at the vicinity of Pd particles.

Observing the cross-sectional images in Fig. 3a and b, the initially deposited NiP particles were sparsely dispersed on the substrate and then the deposit became dense and covered all the surface of substrate gradually as the deposition proceeded. The number of the deposited NiP particle is clearly increasing as the deposition time increasing. In Fig. 3b, the size of the deposited particles is approximately 5–10 nm. These results are the same as shown in Fig. 4a and b. There is a larger amount of fine NiP particles deposited between the original particles in the deposits for 4 s. Fig. 5b is the EDS spectrum detected in some places of the deposits for 4 s. It reveals that these places in deposits consist mainly of Ni and have no Pd appeared in which. The beam size of the EDS analysis is about 25 nm and the average particle size of the NiP particles is smaller than 10 nm. We can infer that the

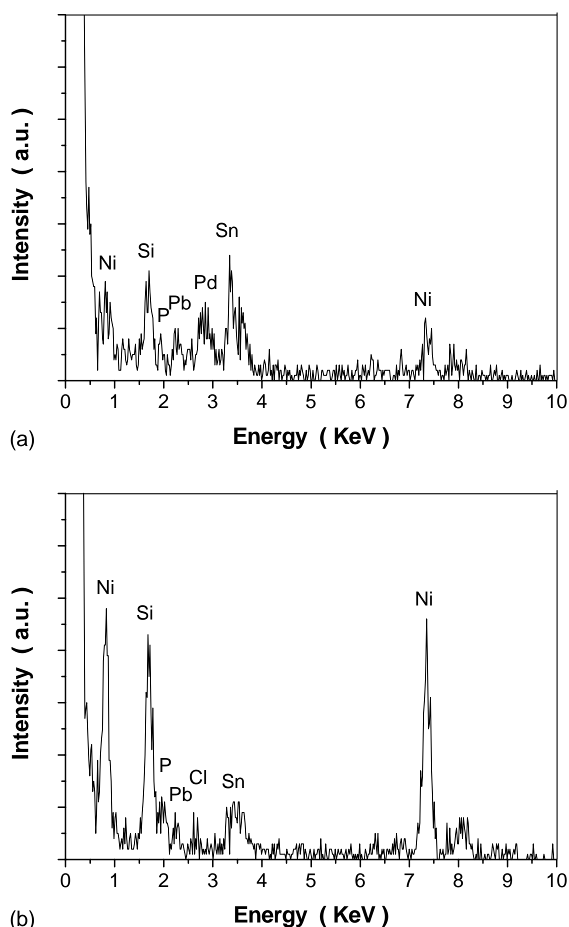

Fig. 5. EDS spectra of the deposits deposited at pH 5.2 plating for: (a) 2 s; and (b) 4 s.

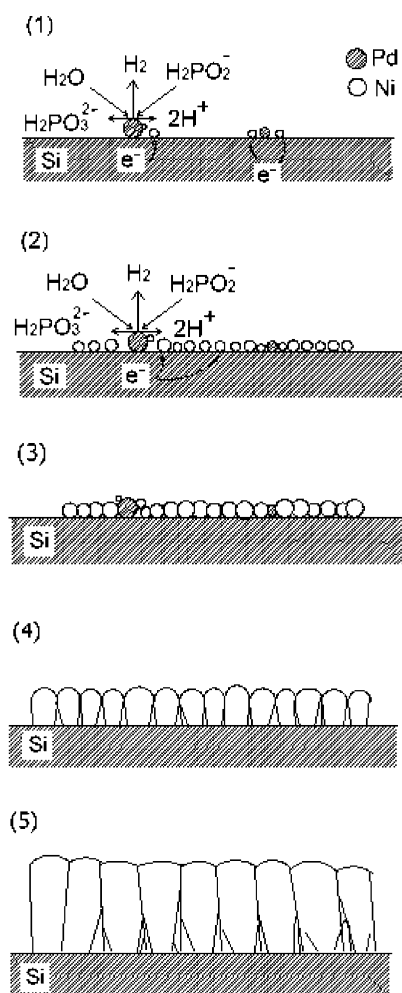

Fig. 6. Schematic of the growth process for the electroless NiP deposited on Si substrate pretreated by $SnCl_2$/HCl and $PdCl_2$/HCl solutions.

deposition of NiP is nucleated not only on the Pd particles but also between the Pd particles from these observations. The result is divergent from the observations of Marton and Schlesinger [23] and Severin et al. [24]. They concluded that the growth of NiP starts only on Pd particle basely on the chemical reduction mechanism. However, Hwang and Lin [25] who investigated the nucleation and growth of electroless CoP on HOPG with AFM had a similar result as our observations and concluded the reaction mechanism appears to be an electrochemical mechanism.

In Fig. 3c, the average thickness of the deposit for 6 s is approximately 20 nm. The deposited particles grew and coalesced together and the deposits became denser than the deposits for 4 s. This observation is confirmed by the surface micrograph of the deposits for 6 s, as is seen in Fig. 4c. The increasing in size and decreasing in number of NiP particle mean that the NiP particle gradually grew and coalesced in this deposition stage.

Fig. 3d and e is the TEM cross-sectional image of the deposits for 15 and 60 s, respectively. It is clear that the deposits are composed of a columnar structure grown in the vertical direction of the substrate surface. When the deposits become dense and continuous on the substrate surface, there are no spaces for the growth of the deposited NiP particles in the horizontal direction of the substrate surface. The deposits grow only in the vertical direction of the substrate surface,

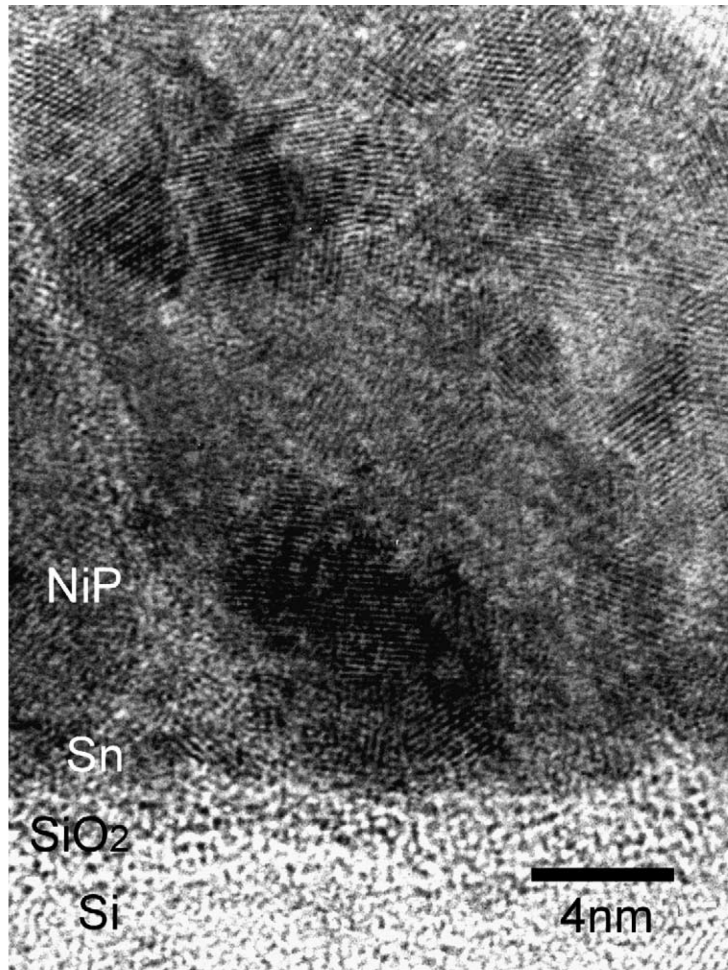

Fig. 7. Lattice image of the as-deposited electroless Ni–P alloy deposited at pH 5.2 characterized by HRTEM.

because the growth in the horizontal direction is limited. As the deposition proceeded, the columns continuous grew along the vertical direction and coalesced by combining small columns to fewer thicker columns. Fig. 4d and e presents the corresponding surface micrograph of deposit for 15 and 60 s, respectively. These are typical surface morphology of the electroless NiP deposits. These semispherical convexes on the surface of deposit are terminals of columnar structure. The convexes tend to increase in size with prolongation of the deposition duration is the result of the coalescence of columns.

The column structure is also appeared in the deposits plating at pH 4.8 and 4.2. The average phosphorus content of pH 4.8 and 4.2 is 15.2 and 20.3 at.%, respectively. These results show that the growth morphology of deposit was not affected by the phosphorus content in deposit or the pH value of plating solution. The column growth of the electroless NiP on Si substrate is distinct from the conventional lamination growth reported by Brenner and Riddell [1], Marton and Schlesinger [23], and Homma et al. [26]. They studied the growth of the electroless NiP on various dielectric substrates pretreated by $SnCl_2$/HCl and $PdCl_2$/HCl.

Fig. 6 shows the possible growth morphology for the electroless NiP deposited on Si substrate pretreated by $SnCl_2$/HCl and $PdCl_2$/HCl solutions. The growth process can be summed up to five steps as follows.

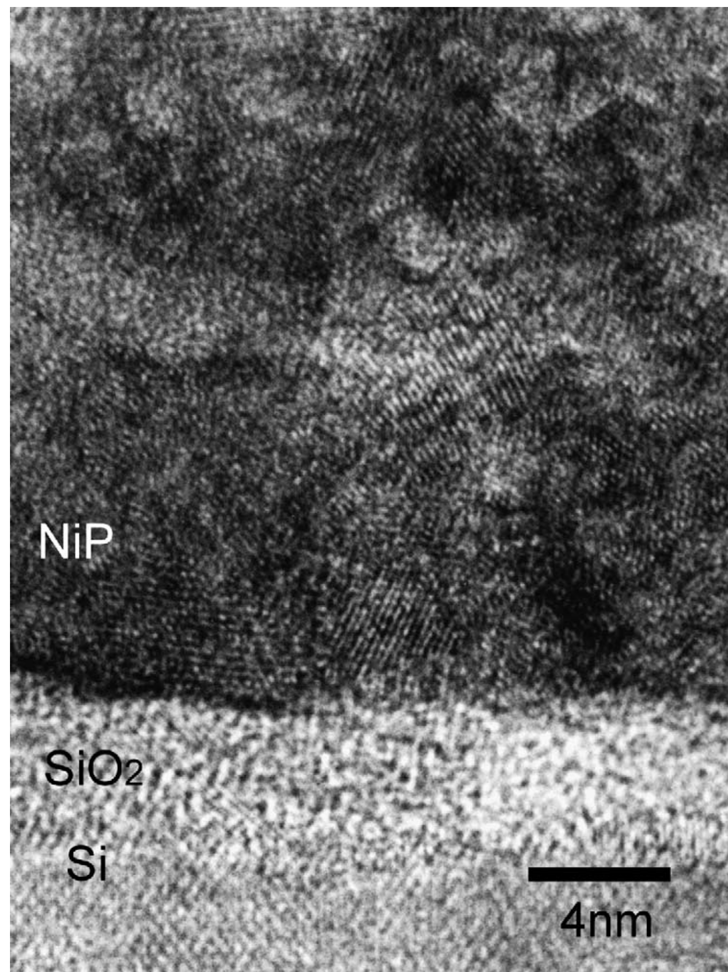

Fig. 8. Lattice image of the as-deposited electroless Ni–P alloy deposited at pH 4.8 characterized by HRTEM.

(1) The NiP particles began to deposit at the vicinity of the Pd particles in the initial deposition stage.
(2) Large amount of new fine NiP particles are nucleated not only near the Pd particles but also between the Pd particles and the original NiP particles grow simultaneously.
(3) The deposited NiP particles grew and coalesced together and the deposits became continuous and denser.
(4) The deposited particles continue grow and exhibited column form grown in the vertical direction of the substrate surface, as the deposition proceeded.
(5) In final, the columns continue grow along the vertical direction and coalesce into thicker columns.

3.3. Crystallinity

In spite of many studies [27–30] devoted to the crystallization of the electroless NiP, no consensus has been reached on the crystallinity of the electroless NiP deposits. The conventional techniques for determining the crystallinity of electroless NiP are electron and X-ray diffraction. These methods are short of the direct evidences to distinguish the amorphous or nanocrystal in the deposits. Also any minor precipitate with small volume fraction may not be detected by X-ray diffraction. In the present study, we observed the crystallinity of the as-deposited electroless NiP film directly using the lattice image characterized by HRTEM.

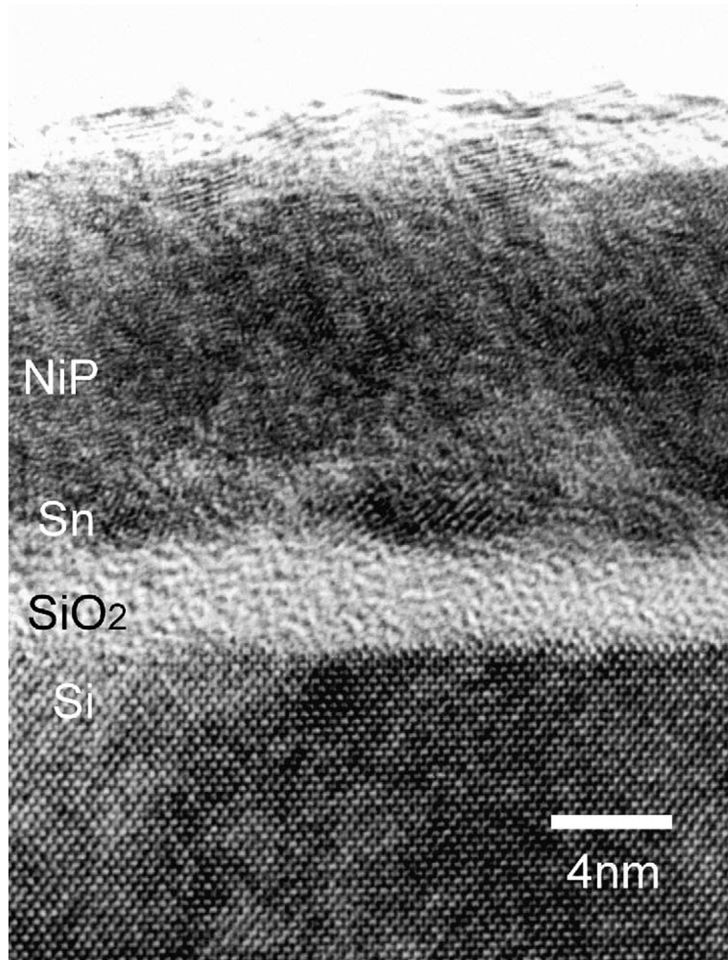

Fig. 9. Lattice image of the as-deposited electroless Ni–P alloy deposited at pH 4.2 characterized by HRTEM.

Fig. 7 shows the lattice image of the as-deposited electroless NiP film deposited at pH 5.2. The phosphorus content of the NiP deposit is approximately 10.7 at.%. As is described above, there is an amorphous SiO_2 layer of which thickness is about 2–3 nm between the Si substrate and the sensitization layer (labeled as Sn). The sensitization layer became discontinuous in the deposition process, so we cannot find the sensitization layer at some place between the NiP deposit and the SiO_2 layer in the lattice images. It is obvious that the NiP deposit with 10.7 at.% P possesses good crystallinity. There are many nanocrystals about 4–8 nm distributed randomly in the deposit. The *d* space of the nanocrystals was measured about 2.03 Å. The value of *d* space conforms to the (1 1 1) of fcc Ni. It indicates that these nanocrystals are pure Ni.

Figs. 8 and 9 are the lattice images of the as-deposited NiP deposited at pH 4.8 and 4.2, respectively. The phosphorus contents of these NiP alloy deposits are 15.2 and 20.3 at.%, respectively. The size of order range in the NiP film deposited at pH 4.8, as shown in Fig. 8, is smaller than the size at pH 5.2. The grain sizes of these nanocrystals were measured about 2–5 nm. In Fig. 9, it is clear that the size of order range in the deposits at pH 4.2 is smaller than in deposits at pH 5.2 and 4.8. The lattice image of the electroless NiP deposited at pH 4.2 is unlike the amorphous morphology of the SiO_2, although the grain sizes of these nanocrystals are under 1.5 nm. It means the deposit with 20.3 at.% phosphorus content is still consisted of nanocrystalline and not amorphous as discussed in the previous papers [27,29,30].

These observations of lattice image also confirm that the grain size of the as-deposited electroless NiP decreases as the phosphorus content increases. We know the phosphorus atom has zero solubility in the nickel lattice from the phase diagram and the nanocrystals in deposits are pure Ni confirmed by the *d* space measurement. It seems reasonable to conclude the phosphorus atoms gather around the deposited Ni nanocrystals in the deposition process. As the phosphorus content is increased, the size of order range or the grain size of Ni crystal is decreased. Hentschel et al. [31] also agree with our conclusion in their report investigating the distribution of P in as-plating electroless NiP.

4. Conclusion

In this paper, we made a thorough study about the growth morphology and crystallinity of electroless NiP alloy containing 10.7–20.3 at.% phosphorus content deposited on silicon wafer sensitized by $SnCl_2$ and activated by $PdCl_2$. The reaction mechanism of the electroless NiP deposited on Si appears to be an electrochemical mechanism and the deposits are composed of a columnar structure grown along the vertical direction of the substrate surface. The phosphorus content does not have influence on the growth morphology but affects the crystallinity of the deposits. The observations of lattice image show the grain size decreases as the phosphorus content increases. The as-deposited NiP alloy with 10.7 at.% P possesses good crystallinity and consists of Ni nanocrystals about 4–8 nm distributed randomly in the deposits. The sizes of nanocrystals in the deposits with 15.2 at.% P were measured about 2–5 nm. The deposits with 20.3 at.% P have a lower degree of order and the size of nanocrystal is under 1.5 nm.

Acknowledgements

The authors gratefully acknowledge research assistance by Wei-Long Liu, Wen-Jauh Chen, and Shu-Hue Hsieh.

References

[1] A. Brenner, G.E. Riddell, J. Res. NBS 37 (1) (1946) 31.
[2] M.D. Feldstein, Plat. Surf. Fin. 85 (1998) 248.
[3] X. Haowen, Z. Bangwei, J. Mater. Prog. Technol. 124 (2002) 8.
[4] H. Iwasa, M. Yokozawa, I. Teramoto, J. Electrochem. Soc. 115 (1968) 485.
[5] H. Cachet, M. Froment, E. Souteyrand, J. Electrochem. Soc. 139 (1992) 2920.
[6] M.V. Sullivan, J.H. Eigler, J. Electrochem. Soc. 104 (1957) 226.
[7] C.H. Ting, M. Paunovic, P.L. Pai, G. Chiu, J. Electrochem. Soc. 136 (1989) 462.
[8] R.M. Kennedy, K. Minten, X. Yang, D.F. Evans, J. Vac. Sci. Technol. B 9 (1991) 735.
[9] J. Lohau, S. Friedrichowski, G. Dumpich, E.F. Wassermann, J. Vac. Sci. Technol. B 16 (1998) 77.
[10] H. Sugimura, N. Nakagiri, Thin Solid Films 281–282 (1996) 572.
[11] T. Tada, T. Kanayama, J. Vac. Sci. Technol. B 16 (1998) 3934.

[12] Y. Shacham-Diamad, Y. Sverdlov, Microelectron Eng. 50 (2000) 525.
[13] B. Singh, R. Mitra, J. Electrochem. Soc. 127 (1980) 2578.
[14] P.A. Don, G. Popovici, D. Dascalu, Gh. Brezeanu, Al. Popa, J. Electrochem. Soc. 130 (1983) 2472.
[15] J.E. Lynch, P.E. Pehrsson, D.N. Leonard, J.M. Calvert, J. Electrochem. Soc. 144 (1997) 1698.
[16] J.F. Rohan, G. O'Riordan, J. Boardman, Appl. Surf. Sci. 185 (2002) 289.
[17] K.L. Lin, C.L. Chen, J. Electrochem. Soc. 147 (2000) 2604.
[18] J. Wang, X. Fei, Z. Yu, G. Zhao, Appl. Surf. Sci. 84 (1995) 383.
[19] K. Kordás, J. Remes, S. Leppävuori, Appl. Surf. Sci. 178 (2001) 93.
[20] N. Takano, D. Niwa, T. Yamada, T. Osaka, Electrochim. Acta 45 (2000) 3263.
[21] D. Niwa, N. Takano, T. Yamada, T. Osaka, Electrochim. Acta 48 (2003) 1295.
[22] T.K. Tsai, C.C. Chuang, C.G. Chao, W.L. Liu, Diamond Relat. Mater. 12 (2003) 1453.
[23] J.P. Marton, M. Schlesinger, J. Electrochem. Soc. 115 (1968) 16.
[24] J.W. Severin, R. Hokke, H. van der Wel, G. de With, J. Electrochem. Soc. 140 (1993) 682.
[25] B.J. Hwang, S.H. Lin, J. Electrochem. Soc. 142 (1995) 3749.
[26] T. Homma, K. Naito, M. Takai, T. Osaka, Y. Yamazaki, T. Namikawa, J. Electrochem. Soc. 138 (1991) 1269.
[27] A.W. Goldenstein, W. Rostoker, F. Schossberger, G. Gutzeit, J. Electrochem. Soc. 104 (1957) 104.
[28] A.H. Graham, R.W. Lindsay, J. Read, J. Electrochem. Soc. 112 (1965) 401.
[29] S.V.S. Tyagi, V.K. Tandon, S. Ray, Z. Metallkde. 76 (1985) 492.
[30] K.H. Hur, J.H. Jeong, D.N. Lee, J. Mater. Sci. 25 (1990) 2573.
[31] T. Hentschel, D. Isheim, R. Kirchheim, F. Mûller, H. Kreye, Acta Mater. 48 (2000) 933.